Solution of the Orr-Sommerfeld equation on a calculator

By M. J. P. Hack

1. Motivation and objectives

Nearly five decades ago, Orszag (1971) applied an expansion in terms of Chebyshev polynomials to the accurate solution of the Orr-Sommerfeld eigenvalue problem. The work delineated the advantages of spectral methods in the context of linear stability analysis, and compared results to those of the earlier finite-difference based studies by Thomas (1953) and Nachtsheim (1964). In particular, the spectral approach enabled the convergence of the critical Reynolds number of Poiseuille flow, and the first determination of its exact value of $Re_c = 5,772.22$.

The analysis by Orszag (1971) was implemented in the FORTRAN 66 language on the then state-of-the-art Control Data Corporation (CDC) 6600 supercomputer at the National Center for Atmospheric Research. The determination of the eigenvalues of the Orr-Sommerfeld equations applied the original version of the QR algorithm, as outlined by Francis (1961, 1962). The scheme, termed the Francis QR step by Golub & Van Loan (1996), reduces a general matrix to upper Hessenberg form, with subsequent implicit application of a series of shifted QR decompositions.

Advances in the fabrication and design of microchips have led to remarkable increases in their capability, a development well predicted by the now-famous law of Moore (1965). As a consequence, modern integrated circuit chips, such as those serving as central processing units (CPUs) in parallel supercomputers, have typically about 10 million times the number of transistors of the microchips used, for instance, in the CDC 6600. This growth in computing capacity was not limited to top-of-the-range supercomputers, but was mirrored in areas such as personal computers, and calculators. In these areas, economic reasons often favor the re-use of older higher-end chips over the new design of low-range microchips. For example, the Texas Instruments TI-84 Plus CE employed in this work uses an 8-bit Zilog microchip, which was designed in 1976 and became one of the most widely used CPUs in desktop computers in the late 1970s and early 1980s.

Herein we examine whether technological advances during the past 50 years have enabled the reproduction of the solution of a classical eigenvalue problem from the field of linear stability theory, which once required the most powerful and expensive computers available, on one of the cheapest and least powerful computers available at present time, given by a high-school-grade calculator. In Section 2, the Orr-Sommerfeld equation is briefly reviewed, followed by an overview of the Francis QR step in Section 3. The computing hardware is considered in Section 4. Results including convergence and timings are shown in Section 5. The brief ends with a discussion of possible applications in Section 6.

2. Orr-Sommerfeld equation

The Orr-Sommerfeld equation (Orr 1907; Sommerfeld 1908) governs small perturbations in the velocity component normal to the wall in parallel shear flows. Its derivation starts from a decomposition of the fluid velocity vector into a steady base flow and a fluctuating component,

$$\boldsymbol{u}\left(x,y,z,t\right)=\overline{\boldsymbol{u}}\left(x,y,z\right)+\boldsymbol{u'}\left(x,y,z,t\right). \tag{2.1}$$

Non-parallel effects are assumed to be small, so that $\overline{\boldsymbol{u}}=\left(\overline{u}\left(y\right),0,0\right)^{\mathsf{T}}$, where u is the streamwise velocity component, and y is the spatial dimension normal to the wall. The governing equations for small perturbations $\boldsymbol{u'}$ are derived by linearizing the Navier-Stokes equations around the base state. The homogeneity of the base flow in the wall-parallel x and z dimensions and time implies that the coefficients of the governing equations for the perturbations are constant with respect to these coordinates. As a consequence, the application of a Fourier transform in these dimensions leads to decoupled individual harmonics, which is reflected in the normal-mode ansatz,

$$\boldsymbol{u'}\left(x,y,z,t\right)=\hat{\boldsymbol{u}}\left(y\right)\exp\left(\mathrm{i}\left(-\omega t+\alpha x+\beta z\right)\right). \tag{2.2}$$

Here, α and β are the wavenumbers of the perturbations in the streamwise and transverse dimensions, and ω is the perturbation frequency.

The common form of the Orr-Sommerfeld equation is derived by introducing the ansatz Eq. (2.2) into the linearized Navier-Stokes equations and eliminating pressure through the continuity equation, resulting in

$$\left[\left(-\mathrm{i}\omega+\mathrm{i}\alpha\overline{u}\right)\left(\frac{\mathrm{d}^2}{\mathrm{d}y^2}-\alpha^2-\beta^2\right)-\mathrm{i}\alpha\frac{\mathrm{d}^2\overline{u}}{\mathrm{d}y^2}-\frac{1}{Re}\left(\frac{\mathrm{d}^2}{\mathrm{d}y^2}-\alpha^2-\beta^2\right)^2\right]\hat{v}=0. \tag{2.3}$$

The fourth-order ordinary differential equation requires four boundary conditions on $\hat{v}$, which are chosen as

$$\hat{v}|_{y=0}=0, \qquad \hat{v}|_{y=\infty}=0, \tag{2.4}$$

$$\frac{\mathrm{d}\hat{v}}{\mathrm{d}y}|_{y=0}=0, \qquad \frac{\mathrm{d}\hat{v}}{\mathrm{d}y}|_{y=\infty}=0. \tag{2.5}$$

In the temporal stability problem, α and β are prescribed real numbers. In this setting, only certain ω and $\hat{v}$ solve the equation, which gives rise to an eigenvalue problem. The present study applies the stability analysis to plane Poiseuille flow. The base flow is thus given analytically,

$$\bar{u}\left(y\right)=y\left(L-y\right), \tag{2.6}$$

where $L=2$ is the height of the channel.

3. Francis QR step

The present work implements the Francis QR step via implicitly applied complex double shifts. The algorithm is briefly delineated in the following.

The conceptually simplest method for solving the eigenvalue problem,

$$\mathsf{A}\boldsymbol{q}=\lambda\boldsymbol{q}, \tag{3.1}$$

where $\mathsf{A}\in\mathbb{C}^{n\times n}$, is the power iteration, which repeatedly applies the linear operator to the solution vector,

$$\boldsymbol{q}_{k+1} = \mathsf{A}\boldsymbol{q}_k. \tag{3.2}$$

If A is diagonalizable, meaning that it has n linearly independent eigenvectors, a random initial guess, $\boldsymbol{q}_0$, may be expressed as a superposition of these n eigensolutions. The repeated application of A thus converges the solution to the eigenvalue of largest amplitude, λ_1, which decays slower, or amplifies faster, than the remaining eigensolutions. The rate of convergence of the power iteration is given by the ratio of the magnitudes of the first and second eigenvalues of A. Upon computation of the largest eigenvalue, the matrix A can be deflated using Householder reflections, resulting in a modified operator that has the first computed eigenvalue on the first diagonal element with zeros filling the remainder of the first column and ones filling the remainder of the first row. Application of the power iteration to the sub-matrix described by the remaining columns and rows allows successive computation of the full spectrum. From a numerical perspective, this approach is, however, disadvantageous since small errors in the largest eigenvalues may accumulate and thus increasingly undermine the accuracy of the deflation procedure.

A computationally more robust alternative computes all eigenvalues of the operator simultaneously by applying A to n orthogonal vectors that are arranged as the columns of the $n \times n$ matrix Q,

$$\mathsf{Z}_{k+1} = \mathsf{A}\mathsf{Q}_k, \tag{3.3}$$

$$\mathsf{Q}_{k+1}\mathsf{R}_{k+1} = \mathsf{Z}_{k+1}. \tag{3.4}$$

The second row in this iteration scheme describes a QR decomposition of Z_{k+1} into an orthogonal Q_{k+1} and an upper triangular R_{k+1}. If the sequence of Q_k converges to Q, then

$$\mathsf{Q}^{\mathsf{H}}\mathsf{A}\mathsf{Q} = \mathsf{R}, \tag{3.5}$$

implying the Schur decomposition

$$\mathsf{A} = \mathsf{Q}\mathsf{R}\mathsf{Q}^{\mathsf{H}}, \tag{3.6}$$

and the eigenvalues of A are read from the diagonal of R. At the kth step of the iteration, an approximation of this relation is given by

$$\mathsf{A} = \mathsf{Q}_k\mathsf{T}_k\mathsf{Q}_k^{\mathsf{H}}, \tag{3.7}$$

equivalent to

$$\mathsf{A}\mathsf{Q}_k = \mathsf{Q}_k\mathsf{T}_k, \tag{3.8}$$

and thus

$$\mathsf{Q}_{k+1}\mathsf{R}_{k+1} = \mathsf{Q}_k\mathsf{T}_k. \tag{3.9}$$

Left multiplication by $\mathsf{Q}_k^{\mathsf{H}}$ gives

$$\mathsf{U}_{k+1}\mathsf{R}_{k+1} = \mathsf{T}_k, \tag{3.10}$$

where $\mathsf{U}_{k+1} \equiv \mathsf{Q}_k^{\mathsf{H}}\mathsf{Q}_{k+1}$. Hence,

$$\begin{aligned}
\mathsf{T}_{k+1} &= \mathsf{Q}_{k+1}^{\mathsf{H}}\mathsf{A}\mathsf{Q}_{k+1} && (3.11)\\
&= \mathsf{U}_{k+1}^{\mathsf{H}}\mathsf{Q}_k^{\mathsf{H}}\mathsf{A}\mathsf{Q}_k\mathsf{U}_{k+1} && (3.12)\\
&= \mathsf{U}_{k+1}^{\mathsf{H}}\mathsf{T}_k\mathsf{U}_{k+1} && (3.13)\\
&= \mathsf{R}_{k+1}\mathsf{Q}_{k+1}. && (3.14)
\end{aligned}$$

It is thus possible to immediately evaluate T_{k+1} from T_k without the orthogonal factors in the orthogonal iteration. Specifically, the algorithm

$$\begin{aligned}
\mathsf{U}_k\mathsf{R}_k &= \mathsf{T}_k, && (3.15)\\
\mathsf{T}_{k+1} &= \mathsf{R}_k\mathsf{U}_k, && (3.16)
\end{aligned}$$

defines the QR iteration. Nevertheless, a naive implementation of the QR iteration, starting, for instance, from $\mathsf{U}_0 = \mathsf{I}$, is ineffective as each step requires a QR factorization of a full matrix, which entails a computational cost of $O(n^3)$. Suppose that, instead, U_0 implements a similarity transformation so that

$$\mathsf{H} = \mathsf{U}_0^{\mathsf{H}}\mathsf{A}\mathsf{U}_0, \tag{3.17}$$

where H is upper Hessenberg with $\mathsf{H}_{ij} = 0$ for $i > j+1$. In this setting, the QR decomposition of H only requires the elimination of a single non-zero element below the diagonal in each column, which reduces the computational cost of each step of the iteration from $O(n^3)$ for an arbitrary A to $O(n^2)$. Furthermore, the QR decomposition of H leads to a Q which is again Hessenberg, implying that the product RQ is also Hessenberg. It follows that with the exception of the initial QR decomposition, the remaining steps of the scheme entail a cost of $O(n^2)$. This scheme is known as the Hessenberg QR step.

Similar to the classic QR factorization, the initial U_0 can be found as a sequence of Givens rotations or Householder reflections. The conceptually simple approach of identifying U_0 via the Gram-Schmidt process is usually avoided owing to its limited numerical stability. In the following, we briefly describe the Householder reflection, which transforms the operand vector $\boldsymbol{x}$ into a direction parallel to a prescribed unit vector, $\boldsymbol{y}$, so that

$$\mathsf{P}\boldsymbol{x} = \|\boldsymbol{x}\|_2\boldsymbol{y}. \tag{3.18}$$

The operation is implemented via a reflection through a hyperplane that bisects the angle between $\boldsymbol{x}$ and $\boldsymbol{y}$. The specific choice $\boldsymbol{y} = \boldsymbol{e}_1$ eliminates all but the first element of vector $\boldsymbol{x}$. For real vectors $\boldsymbol{x} \in \mathbb{R}^{n\times 1}$, an explicit form of P is found by observing

$$\begin{aligned}
\|\boldsymbol{x}\|_2\boldsymbol{y} =& \boldsymbol{x} - (\boldsymbol{x} - \|\boldsymbol{x}\|_2\boldsymbol{y}) && (3.19)\\
=& \boldsymbol{x} - \frac{2\left(\boldsymbol{x} - \|\boldsymbol{x}\|_2\boldsymbol{y}\right)\left(\boldsymbol{x}^{\mathsf{T}}\boldsymbol{x} - \|\boldsymbol{x}\|_2\boldsymbol{y}^{\mathsf{T}}\boldsymbol{x}\right)}{2\|\boldsymbol{x}\|_2^2 - 2\|\boldsymbol{x}\|_2\boldsymbol{y}^{\mathsf{T}}\boldsymbol{x}} && (3.20)\\
=& \boldsymbol{x} - \frac{2\left(\boldsymbol{x} - \|\boldsymbol{x}\|_2\boldsymbol{y}\right)\left(\boldsymbol{x}^{\mathsf{T}} - \|x\|_2\boldsymbol{y}^{\mathsf{T}}\right)\boldsymbol{x}}{2\|\boldsymbol{x}\|_2^2 - 2\|\boldsymbol{x}\|_2\boldsymbol{y}^{\mathsf{T}}\boldsymbol{x}} && (3.21)\\
=& \boldsymbol{x} - 2\frac{\boldsymbol{u}\boldsymbol{u}^{\mathsf{T}}\boldsymbol{x}}{\|\boldsymbol{u}\|_2^2} && (3.22)\\
=& \left(\mathsf{I} - 2\frac{\boldsymbol{u}\boldsymbol{u}^{\mathsf{T}}}{\|\boldsymbol{u}\|_2}\right)\boldsymbol{x} && (3.23)\\
\equiv& \mathsf{P}\boldsymbol{x}. && (3.24)
\end{aligned}$$

Here, the square of the 2-norm of $\boldsymbol{u}$ is,

$$\begin{aligned}\|\boldsymbol{u}\|_2^2 =& \left(\boldsymbol{x} - \|\boldsymbol{x}\|_2\boldsymbol{y}\right)^{\mathsf{T}}\left(\boldsymbol{x} - \|\boldsymbol{x}\|_2\boldsymbol{y}\right) && (3.25)\\ =&\|\boldsymbol{x}\|_2^2 - 2\|\boldsymbol{x}\|_2\boldsymbol{x}^{\mathsf{T}}\boldsymbol{y} + \|\boldsymbol{x}\|_2\|\boldsymbol{y}\|_2 && (3.26)\\ =&2\|\boldsymbol{x}\|_2^2 - 2\|\boldsymbol{x}\|_2\boldsymbol{y}^{\mathsf{T}}\boldsymbol{x}, && (3.27)\end{aligned}$$

with the last row following from $\|\boldsymbol{y}\|_2 \equiv 1$. In the complex case, $\boldsymbol{x} \in \mathbb{C}^{n\times 1}$, with $\boldsymbol{y} = \boldsymbol{e}_1$, the above choice of P yields

$$\mathsf{P}\boldsymbol{x} = -\operatorname{sgn}(x_1)\|\boldsymbol{x}\|_2\boldsymbol{e}_1, \qquad (3.28)$$

where x_1 is the first element of $\boldsymbol{x}$, and sgn is the sign function, which for a complex argument returns the exponential of the phase,

$$\begin{aligned}\operatorname{sgn}(z) =& \frac{z}{|z|} && (3.29)\\ =& \exp(\mathrm{i}\varphi), && (3.30)\end{aligned}$$

with $\varphi = \operatorname{atan2}(\operatorname{Real}(z), \operatorname{Imag}(z))$. The initial transform of A into Hessenberg H may thus be expressed as

$$\mathsf{U}_0 = \mathsf{P}_1\mathsf{P}_2\cdots\mathsf{P}_{n-2}, \qquad (3.31)$$

with unitary $\mathsf{P}_j \equiv \mathsf{I} - 2c\boldsymbol{v}\boldsymbol{v}^{\mathsf{H}}$. This initial reduction of A to Hessenberg form requires a single step, at cost of $O(n^3)$.

While the Hessenberg QR step iterates at reduced cost compared to the QR iteration, the rate of convergence is the same as in the original orthogonal iteration. Specifically, the error in the p-th eigenvalue of H converges to zero at the rate

$$|\frac{\lambda_{p+1}}{\lambda_p}|. \qquad (3.32)$$

In what is known as the Francis QR step, the convergence of the iteration scheme is improved by applying a shift μ to the operator,

$$\begin{aligned}\mathsf{U}_k\mathsf{R}_k =& \mathsf{T}_k - \mu\mathsf{I}, && (3.33)\\ \mathsf{T}_{k+1} =& \mathsf{R}_k\mathsf{U}_k + \mu\mathsf{I}. && (3.34)\end{aligned}$$

In this case, the convergence rate of pth column becomes $|\lambda_{p+1} - \mu|/|\lambda_p - \mu|$. If μ is an eigenvalue of H, then $\mathsf{H}-\mu\mathsf{I}$ is singular, and the last row of R is zero. As a consequence, the last row of the product $\mathsf{T}_{k+1} = \mathsf{R}_k\mathsf{U}_k$ is zero as well. The matrix T_{k+1} has thus become a reduced Hessenberg matrix, with μ on the diagonal of column $n-1$ and $h_{n,n-1} = 0$. In the more realistic case where μ approximates an eigenvalue of H, $h_{n,n-1}$ is small and $h_{n,n} \approx \mu$. In this setting, the choice of $h_{n,n}$ as the new shift generally causes $h_{n,n-1}$ to converge to zero quadratically.

In the case of complex eigenvalues of the submatrix $\mathsf{H}_{(n-1:n,n-1:n)}$, the double-shift strategy operating on the two shifts μ_1 and μ_2 is typically applied. In this setting,

$$\begin{aligned}\mathsf{U}_1\mathsf{R}_1 =& \mathsf{H} - \mu_1\mathsf{I}, && (3.35)\\ \mathsf{H}_1 =& \mathsf{R}_1\mathsf{U}_1 + \mu_1\mathsf{I}, && (3.36)\\ \mathsf{U}_2\mathsf{R}_2 =& \mathsf{H}_1 - \mu_2\mathsf{I}, && (3.37)\\ \mathsf{H}_2 =& \mathsf{R}_2\mathsf{U}_2 + \mu_2\mathsf{I}. && (3.38)\end{aligned}$$

Specifications	**CDC 6600**	**TI-84 Plus CE**
Base language	FORTRAN 66	TI-BASIC
Price at release	\$2,300,000	\$99.95
Power supply	30 kW @208 V	Rechargeable
CPU	Custom design @10 MHz	Zilog eZ80 @48 MHz
Total system memory	65,000 60-bit words	154 kB

Table 1. Comparison of key attributes of the Texas Instruments TI-84 Plus and Control Data CDC 6600.

It can be shown that

$$(\mathsf{U}_1\mathsf{U}_2)\,(\mathsf{R}_1\mathsf{R}_2) = \mathsf{M} \tag{3.39}$$

is a QR factorization of $\mathsf{M} = (\mathsf{H} - \mu_1\mathsf{I})\,(\mathsf{H} - \mu_2\mathsf{I})$. The evaluation of M via the evaluation of H^2 however entails a cost of $O(n^3)$ and is thus impractical. The Francis QR step therefore employs the so-called double-implicit-shift strategy which makes use of the Implicit Q Theorem which states that if $\mathsf{Z}^\mathsf{T}\mathsf{H}\mathsf{Z}$ and $\mathsf{Z}_1^\mathsf{T}\mathsf{H}\mathsf{Z}_1$ are both unreduced Hessenberg matrices without zeros in the subdiagonal, then the first columns of Z and Z_1 are the same. In this setting, it is possible to obtain H_2 implicitly by evaluating only the first column of M and determining a Householder matrix P_0 that transforms the first column of M into a multiple of $\boldsymbol{e}_1$.

4. Hardware

As part of this project, the Francis QR step has been implemented on a TI-84 Plus CE calculator by Texas Instruments. The calculator is limited in its capabilities owing to its SAT certification. The device allows a limited range of linear algebra operations, including the computation of the determinant of a matrix, as well as the computation of inverses. Up to eight matrices can be kept in memory, each of which is restricted to a size of 20 × 20 elements. Critically, matrices only support real entries so that two matrices must be used to represent a complex operator. Sparse operators are not specifically supported, but can be conceptually implemented by the user via a reinterpretation of the entries of the matrices. Doing so would, for instance, allow the use of a 20 × 20 operator in a fourth-order finite-difference discretization based on a five-point stencil of a one-dimensional domain using 80 grid points. As outlined above, the present work instead follows Orszag (1971) in discretizing the wall-normal coordinate of the physical domain using Chebyshev polynomials, which leads to dense operators.

Beyond the very limited set of built-in operations, the TI-84 Plus CE also supports the implementation of arbitrary operations in the TI-BASIC language which was used in the present work. Since TI-BASIC is an interpreted language, it entails considerable performance disadvantages compared to compiled code. It should be noted that the TI-84 can alternatively be programmed at machine-code level using assembly language. A comparison of key attributes of the TI-84 Plus CE and the CDC 6600 computer is presented in Table 1.

Resolution	Eigenvalue	Relative error
$N = 8$	$\omega = 0.6609 - 0.0050\mathrm{i}$	$D = 137.23\%$
$N = 12$	$\omega = 0.3436 - 0.0047$	$D = 23.35\%$
$N = 16$	$\omega = 0.2675 - 0.0097\mathrm{i}$	$D = -3.90\%$
$N = 20$	$\omega = 0.2748 - 0.0057\mathrm{i}$	$D = -1.35\%$
$N = 100$	$\omega_{\mathrm{ref}} = 0.2785 - 0.0049\mathrm{i}$	$D = 0$

TABLE 2. Comparison of computed least stable eigenvalues as a function of the number of Chebyshev polynomials, N.

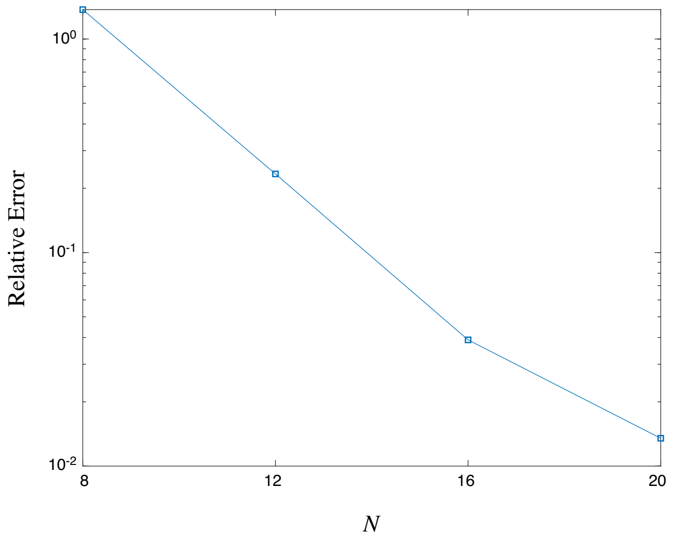

FIGURE 1. Convergence of the first eigenvalue. Relative error as a function of the number of Chebyshev polynomials, N.

5. Results

The following results were computed for a Reynolds number based on the channel half-height of $Re = 4,000$, and streamwise and transverse wavenumbers $\alpha = 1$ and $\beta = 0$, respectively. The least stable eigenvalue is given in Table 2 for three different resolutions, and compared to the converged result obtained for $N = 100$ on a desktop workstation. The third column gives the relative error, $(|\omega| - |\omega_{\mathrm{ref}}|)/\omega_{\mathrm{ref}}$. Overall, these results show that the first eigenvalue is reasonably well approximated for the largest supported number of grid points, $N = 20$. As expected from a spectral discretization method, the convergence rate is exponential, as visualized in Figure 1.

In addition, we also consider the timing of the solution procedure. The scaling of the complexity of the algorithm implies that the computational cost is proportional to the third power of N. The timings for the individual cases are presented in Figure 2. The resulting distribution is consistent with the $O\left(n^3\right)$ cost of the algorithm as indicated by the dashed line representing a third-order polynomial.

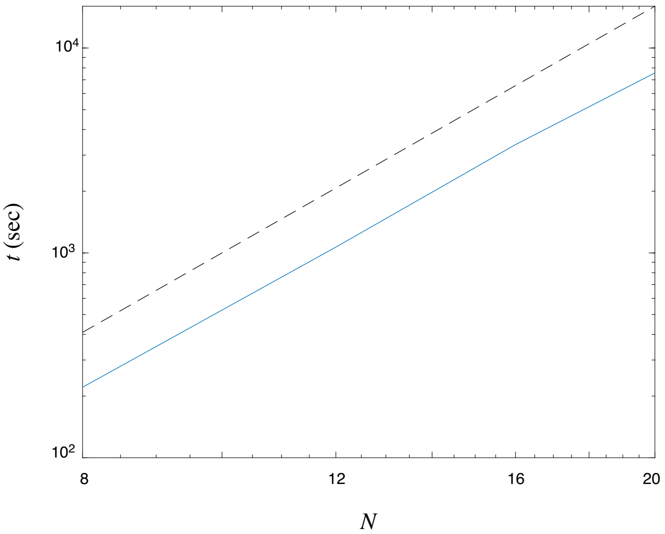

FIGURE 2. Timings of the solution of the eigenvalue problem for different resolutions (solid), third-order polynomial (dashed).

6. Conclusion and outlook

The Orr-Sommerfeld eigenvalue problem has been solved by implementing the Francis QR step on a programmable calculator. The least stable eigenvalue has been computed to a precision that would make the approach useful in the context of active control applications. A convergence analysis confirmed the exponential decay of the error in the first eigenvalue. The wall-clock time required for the solution was shown to grow cubically with problem size.

Linear stability theory is a valuable reduced-order tool that, for instance, enables the study of the mechanisms driving transition to turbulence with moderate computational effort. Linear models also play an important role in the prediction of transition to turbulence as well as in model-driven active control. In these settings, an instantaneous evaluation of the stability of the flow based on the solution of the stability problem has the potential to enhance the fidelity of the predictions in comparison to data-driven approaches. The computational resources available as part of an active control setup are nonetheless considerably less than those commonly used in scientific studies. This study shows that high-fidelity modeling and control approaches can be realized on limited hardware.

REFERENCES

FRANCIS, J. G. F. 1961 The QR transformation. Part 1. *Comput. J.* **4**, 265–271.

FRANCIS, J. G. F. 1962 The QR transformation. Part 2. *Comput. J.* **4**, 332–345.

GOLUB, G. H. & VAN LOAN, C. F. 1996 *Matrix Computations*, 3rd edition, The Johns Hopkins University Press, Baltimore.

MOORE, G. E. 1965 Cramming more components onto integrated circuits. *Electronics* **38**, 114–117.

NACHTSHEIM, P. R. 1964 An initial value method for the numerical treatment of the

Orr-Sommerfeld equation for the case of plane Poiseuille flow. *NASA Tech. Note* D-2414.

Orr, W. M. F. 1907 The stability or instability of the steady motions of a perfect liquid and of a viscous liquid. Part I: A perfect liquid. Part II: A viscous liquid. *Proc. R. Irish Acad. A* **27**, 9–138.

Orszag, S. A. 1971 Accurate solution of the Orr-Sommerfeld stability equation. *J. Fluid Mech.* **50**, 689–703.

Sommerfeld, A. 1908 Ein Beitrag zur hydrodynamischen Erklärung der turbulenten Flüssigkeitbewegungen. In *Atti. del 4. Congr. Internat. dei Mat. III*, pp. 116–124.

Thomas, L. H. 1953 The stability of plane Poiseuille flow. *Phys. Rev.* **91**, 780–783.